Medium Depth Influences O_2 Availability and Metabolism in Human RPE Cultures

Daniel T. Hass,[1] Qitao Zhang,[2] Gillian A. Autterson,[2] Richard A. Bryan,[3] James B. Hurley,[1] and Jason M. L. Miller[2,4]

[1]Department of Biochemistry, The University of Washington, Seattle, Washington, United States
[2]Kellogg Eye Center, University of Michigan, Ann Arbor, Michigan, United States
[3]Lucid Scientific, Atlanta, Georgia, United States
[4]Cellular and Molecular Biology Program, University of Michigan, Ann Arbor, Michigan, United States

Correspondence: Jason M. L. Miller, Kellogg Eye Center, University of Michigan Office 7107, Brehm Tower, 1000 Wall Street, Ann Arbor, MI 48105, USA;
miljason@umich.edu.

DTH and QZ contributed equally to this article.

Received: May 14, 2023
Accepted: October 13, 2023
Published: November 3, 2023

Citation: Hass DT, Zhang Q, Autterson GA, Bryan RA, Hurley JB, Miller JML. Medium depth influences O_2 availability and metabolism in human RPE cultures. *Invest Ophthalmol Vis Sci.* 2023;64(14):4. https://doi.org/10.1167/iovs.64.14.4

Purpose. Retinal pigment epithelium (RPE) oxidative metabolism is critical for normal retinal function and is often studied in cell culture systems. Here, we show that conventional culture media volumes dramatically impact O_2 availability, limiting oxidative metabolism. We suggest optimal conditions to ensure cultured RPE is in a normoxic environment permissive to oxidative metabolism.

Methods. We altered the availability of O_2 to human primary and induced pluripotent stem cell–derived RPE cultures directly via a hypoxia chamber or indirectly via the amount of medium over cells. We measured oxygen consumption rates (OCRs), glucose consumption, lactate production, $^{13}C_6$-glucose and $^{13}C_5$-glutamine flux, hypoxia inducible factor 1α (HIF-1α) stability, intracellular lipid droplets after a lipid challenge, transepithelial electrical resistance, cell morphology, and pigmentation.

Results. Medium volumes commonly employed during RPE culture limit diffusion of O_2 to cells, triggering hypoxia, activating HIF-1α, limiting OCR, and dramatically altering cell metabolism, with only minor effects on typical markers of RPE health. Media volume effects on O_2 availability decrease acetyl-CoA utilization, increase glycolysis and reductive carboxylation, and alter the size and number of intracellular lipid droplets under lipid-rich conditions.

Conclusions. Despite having little impact on visible and typical markers of RPE culture health, media volume dramatically affects RPE physiology "under the hood." As RPE-centric diseases like age-related macular degeneration involve oxidative metabolism, RPE cultures need to be optimized to study such diseases. We provide guidelines for optimal RPE culture volumes that balance ample nutrient availability from larger media volumes with adequate O_2 availability seen with smaller media volumes.

Keywords: retinal pigment epithelium, oxygen, metabolism, isotopic labeling, glucose, lactate, ketone bodies, β-hydroxybutyrate, hypoxia, mitochondria, lipid droplets

In the vertebrate eye, the retinal pigment epithelium (RPE) is a cell monolayer that supports photoreceptor health.[1–3] The RPE is wedged between photoreceptors on its apical surface and a high-flow, fenestrated capillary bed called the choriocapillaris on its basolateral surface. The RPE is the primary site of degeneration in common blinding eye diseases, including Stargardt disease and age-related macular degeneration (AMD). Numerous lines of evidence support the importance of mitochondrial metabolism in RPE homeostasis: (1) the RPE is among the first tissues in the body affected in inherited mitochondrial disorders,[4,5] (2) defects in RPE mitochondrial function result in proximal photoreceptor degeneration,[6] and (3) RPE degeneration in AMD is marked by significant mitochondrial structural abnormalities.[7,8] The RPE lives in a synergistic metabolic relationship with overlying photoreceptors, wherein photoreceptors produce lactate and succinate that the RPE consumes.[9,10] RPE mitochondria also consume lipids, which may be derived from phagocytosed photoreceptor outer segments or uptake of circulating lipoprotein particles.[11–13]

Cells use energy from oxidation of fuels and reduction of O_2 to drive ATP synthesis.[14] In the terminal step of the mitochondrial electron transport chain (ETC), cytochrome C oxidase reduces O_2 to H_2O. Without O_2, oxidation of metabolic intermediates upstream of cytochrome C oxidase is limited. Accumulation of reduced redox coenzymes under hypoxia leads to a metabolic shift toward glycolysis and lactate production, which generates energy less efficiently. To ensure an adequate O_2 supply for mitochondria, nearly all animals have evolved circulatory and respiratory systems.

Culture of human primary and induced pluripotent stem cell (iPSC)–derived RPE is used to model RPE-based retinal degenerations.[15–21] An important assumption in these studies is that atmospheric O_2 concentrations do not limit

mitochondrial activity. Estimates in vivo suggest that the fractional O_2 availability at the RPE is ~4% to 9% (30–70 mm Hg),[22] whereas fractional atmospheric O_2 is 21% (160 mm Hg), suggesting RPE in vitro could be in a *hyperoxic* environment. However, O_2 dissolved in media and consumed by cultures must be replaced by diffusion from air above the medium. In accordance with Fick's laws, O_2 flux through the medium is constrained by the distance over which it must diffuse. The circulatory system delivers O_2 continuously to within microns of a cellular target. In culture, O_2 must diffuse across ~3 to 25 mm of media, several orders of magnitude greater than diffusion distances in vivo. If cellular O_2 consumption exceeds O_2 diffusion through culture medium, cells will deplete the medium of O_2 and lose the ability to oxidize fuels.[23,24]

Herein, we test whether O_2 consumption by RPE cultures is greater than diffusion of O_2 into the medium. We use multiple methods to show that widely employed media volumes limit O_2 availability in RPE cultures, stabilize the hypoxia sensor hypoxia inducible factor 1α (HIF-1α), increase glycolysis and promote reductive carboxylation, impair mitochondrial metabolism, and alter intracellular lipid storage. Despite dramatic impacts on metabolism, other markers of RPE health are only subtly changed by prolonged exposure to higher media volumes. Lower media volumes restore O_2 availability and mitochondrial metabolism but also result in faster nutrient depletion. We provide guidelines for how to balance media volumes and media change frequencies to preserve both nutrient availability and mitochondrial metabolism in cultured RPE.

Materials and Methods

Cell Culture and Transepithelial Electrical Resistance

Primary human prenatal RPE cultures (hfRPE) were grown and transepithelial electrical resistance (TEER) measured according to our detailed protocol outlined earlier.[25,26] Human induced pluripotent stem cell–derived RPE cultures (iPSC-RPE) were grown as previously described.[27] All cultures demonstrated robust pigmentation, cobblestone morphology, and high TEER (at least 500 Ω*cm^2 for hfRPE and 300–400 Ω*cm^2 for iPSC-RPE). All cells for metabolism analysis were passage 1, grown on microporous inserts for at least 5 weeks before experimentation (hfRPE on 24-well inserts—Transwells [Corning, Glendale, USA], product 3470, cell growth area of 0.33 cm^2 and iPSC-RPE on 12-well inserts—Transwells [Corning, Glendale, USA], product 3460, cell growth area of 1.12 cm^2). Cells for Resipher experiments were grown on tissue culture–treated plastic in 96-well plates (Falcon [Corning, Glendale, USA], product 353072, cell growth area of 0.32 cm^2) and utilized for experiments only when cells were cobblestone and pigmented. Media compositions are based on standard RPE culture media,[25,26,28,29] with slight variations for each experiment, as outlined in Supplementary Table S1. Media volumes used for 12-well Transwells and 24-well Transwells were adjusted to achieve the same volume to cell culture surface area ratio: apical: 65 µL in 24-well Transwell = 220 µL in 12-well Transwell, 125 µL in 24-well Transwell = 425 µL in 12-well Transwell, 200 µL in 24-well Transwell = 680 µL in 12-well Transwell; basal: 400 µL in 24-well receiver plate = 800 µL in 12-well receiver plate.

Conjugation of Fatty Acids to Bovine Serum Albumin

Sodium palmitate (Sigma, St. Louis, MO, USA; product P9767) or sodium oleate (Sigma; product O7501) fatty acid (FA) was solubilized at 70°C in 150 mM NaCl to create a 12.5-mM solution. The hot 12.5-mM FA solution was transferred to 1.7 mM FA-free BSA (MP Biomedical, Solon, OH, USA; product MP219989910) solubilized in glucose-free α-MEM (Supplementary Table S1) at a ratio of 0.8:1 and stirred at 37°C for 1 hour. The molar concentration of the conjugated FA-BSA solution was then adjusted by addition of 150 mM NaCl for a final concentration of 5 mM FA/0.85 mM BSA (6:1 molar ratio). Our protocol was adapted from Seahorse Bioscience's (Santa Clara, CA, USA) protocol, "Preparation of Bovine Serum Albumin (BSA)-Conjugated Palmitate."

HIF-1α Staining and Hypoxia Chambers

hfRPEs on Transwells were placed in the incubator with either atmospheric O_2 concentrations or in a hypoxia chamber (Embrient Inc., San Diego, CA, USA; product MIC-101) in which O_2 concentration was titrated to 8% utilizing a 1% O_2/5% CO_2/94% N_2 gas mixture and an O_2 sensor (Sensit P100 Personal Gas Leak Monitor; Sensit, Valparaiso, IN, USA) placed within the hypoxia chamber. After 24 hours of exposure, cells were lysed with 40 µL of 1.2× Western blot SDS sample buffer. Within the sample buffer, 100 µM of the prolyl hydroxylase inhibitor DMOG and 10 µM of the protease/phosphatase inhibitor MG-132 (Cell Signaling Technologies, Danvers, MA, USA; product 5872S) were used to prevent degradation of HIF. HIF-1α levels were determined in 25 µg lysate by standard SDS-PAGE and Western blot techniques, utilizing a rabbit anti–HIF-1α antibody (Cell Signaling Technologies, Danvers, MA, USA; product 36169, 1:1000), a mouse monoclonal anti-GAPDH antibody (EnCor product MCA-1D4), and horseradish peroxidase (HRP)–linked secondary antibodies (goat anti-mouse HRP, Jackson ImmunoResearch, West Grove, PA, USA, #115-035-062; donkey anti-rabbit HRP, #711-035-152, Jackson Immuno).

Lipid Loading and Lipid Droplet Staining

hfRPEs or iPSC-RPEs on Transwells were loaded with 300 µM BSA-conjugated palmitate in serum-free media (Supplementary Table S1). Cells were incubated at 37°C for 18 hours and fixed with 4% paraformaldehyde/4% sucrose solution for 15 minutes. After fixation, photochemical bleaching of the samples was performed. First, freshly made bleaching solution (50 µL deionized formamide, 50 µL of 3 M sodium chloride/0.3 M sodium citrate, 800 µL water, 163.4 µL 30% hydrogen peroxide) was added to adequately cover the apical chamber of each Transwell. Next, the liquid light guide of an X-Cite 120Q microscopy system was centered 14 cm over the plate, held in place by a retort stand with a utility clamp. After 2 minutes, Transwells were picked up and tapped gently to dislodge bubbles that formed on the membrane surface. This step was repeated at 5 to 7 minutes. Total bleach time was ~15 to 20 minutes, but duration was slightly altered depending on the degree of pigment visible on the Transwell membrane toward the end of the bleaching process. Postbleaching, Transwells were washed 5 to 8 times with 1× PBS to remove all bubbles. Cells were then quenched with a solution of 50 mM ammonium chloride in

PBS for 10 minutes, permeabilized with 0.01% digitonin in PBS for 30 minutes at room temperature (RT), blocked with 3% BSA in PBS for 20 minutes, and incubated in primary antibody solution (anti-ADRP [perilipin-2], clone AP125 [Progen 610102], 1:10 dilution in 1% BSA in PBS) for 1 hour at RT or overnight at 4°C. Secondary antibody incubations and mounting were done in standard fashion, but avoiding all exposure to detergents. Hoechst-34580 (Sigma 63493, 1:500 dilution) was included in the secondary antibody incubation for 1 hour at RT.

Microscopy

Z-stack images were obtained using the Leica STELLARIS 8 FALCON Confocal Microscope, and image analysis was performed with Aivia 11 (Leica, North Deerfield, IL, USA). To quantify lipid droplets (LDs), a machine learning pixel classifier was trained, with refinement of selected objects using the software's meshes recipe.

Resipher

Resipher (Lucid Scientific, Atlanta, GA, USA) is an instrument that measures oxygen consumption rates (OCR) in standard multiwell culture plates. The device operates by measuring O_2 concentrations across a range of heights in the media above the cell monolayer. These measurements correspond to the O_2 gradient that forms in static media as oxygen diffuses through it. Using these gradient measurements, O_2 flux through the media is calculated using Fick's laws. An introduction to these laws and how they are used is available in the Supplementary Discussion.

Defined volumes of media were placed over cells and OCR was continuously monitored for up to 5 days without media change. Due to known uneven evaporative effects, wells on the edge of the plate were excluded from analysis. Each volume was tested in at least six replicate wells. All wells were confluent with a similar size and number of cells (Supplementary Fig. S1).

Glucose Concentration Assay

We measured media glucose with an enzymatic assay wherein glucose phosphorylation and oxidation was coupled to $NADP^+$ reduction.[30] NADPH absorbs light at 340 nm. We incubated 2 to 5 µL culture medium samples and 2 to 5 µL of 0 to 10 mM standards in the following assay buffer: 50 mM Tris, 1 mM $MgCl_2$, 500 µM $NADP^+$, 500 µM ATP, 0.2 U/mL hexokinase, and 0.08 U/mL glucose-6-phosphate dehydrogenase, pH 8.1. Using a Bio-Tek (Agilent, Santa Clara, CA, USA) Synergy 4 plate reader, we measured A_{340} over time at 37°C until it reached steady state. We used a linear fit of the standard curve to determine glucose concentrations. We determined glucose amount by multiplying concentrations with apical or basal medium volumes. A complete protocol for the glucose assay, including product numbers, is available at dx.doi.org/10.17504/protocols.io.dm6gpj5jdgzp/v1.

Lactate Concentration Assay

We measured media lactate with an enzymatic assay where lactate dehydrogenase converts lactate and NAD^+ to pyruvate and NADH.[30] Pyruvate is consumed by the assay buffer, drawing the reaction to completion. NADH absorbs light at 340 nm. We incubated 2 to 5 µL culture medium samples and 2 to 5 µL of 0 to 20 mM standards in the following assay buffer: 300 mM glycine, 166 mM hydrazine, 2.5 mM NAD^+, and 8 U/mL lactate dehydrogenase. We determined A_{340} at 37°C with a Bio-Tek Synergy 4 plate-reader. Steady-state A_{340} values from standards were used to determine media [lactate]. A complete protocol for the lactate assay, including product numbers, is available at dx.doi.org/10.17504/protocols.io.6qpvr4733gmk/v1.

^{13}C Metabolite Tracing

RPE cells were incubated in culture medium (see Supplementary Table S1 for composition) supplemented with 5 mM $^{13}C_6$-labeled glucose (Cambridge Isotope Laboratories, Tewksbury, MA, USA, CLM-1396-PK) or 2 mM $^{13}C_5$-labeled glutamine (Cambridge Isotope Laboratories, CLM-1822). Conventional medium was exchanged for medium containing ^{13}C-labeled tracers at various apical media volumes (with a constant 400-µL basal volume), and then 20 µL of medium was collected from both the apical side and basal side 4 hours after the medium change for one set of wells and 22 hours after medium change for another set of wells. Collected media were used for downstream analysis of glucose concentration, lactate concentration, and labeling of metabolites with ^{13}C. All experiments contained at least three experimental replicates, with each replicate pooled from at least two different Transwells.

Metabolite Extraction and Derivatization

Metabolites were extracted in 80% MeOH, 20% H_2O supplemented with 10 µM methylsuccinate (Sigma; product M81209) as an internal standard. The extraction buffer was equilibrated on dry ice, and 150 µL was added to 2 µL of each medium sample. Samples were incubated on dry ice for 45 minutes to precipitate protein. Proteins were pelleted at 17,000 × g for 30 minutes at 4°C. The supernatant containing metabolites was lyophilized and stored at −80°C until derivatization.

Lyophilized samples were derivatized with 10 µL of 20 mg/mL methoxyamine HCl (Sigma; product 226904) dissolved in pyridine (Sigma; product 270970) and incubated at 37°C for 90 minutes. Samples were further derivatized with 10 µL tert-butyldimethylsilyl-N-methyltrifluoroacetamide (Sigma; product 394882) and incubated at 70°C for 60 minutes.

Gas Chromatography–Mass Spectrometry

Metabolites were analyzed on an Agilent 7890/5975C GC-MS using methods described extensively in previous work.[31] Briefly, 1 µL of derivatized sample was injected and delivered to an Agilent HP-5MS column by helium gas (1 mL/min). The temperature gradient started at 100°C for 4 minutes and increased 5°C/min to 300°C, where it was held for 5 minutes. We used select ion monitoring (SIM) to record ions (*m/z*: ~50–600) in expected retention time windows. Peaks were integrated in MSD ChemStation (Agilent, Santa Clara, CA, USA). We corrected for natural isotope abundance using IsoCor.[32] Corrected metabolite signals were converted to molar amounts by comparing metabolite peak abundances in samples with those in a standard mix. Multiple concentrations of this mix were extracted, derivatized, and run alongside samples in each experiment.

Sample Nomenclature and Statistical Analysis

Number of donors for experiments is indicated in figure captions. A total of seven hfRPE donors and three iPSC-RPE lines were used for experiments. For all experiments involving mass spectrometry analysis or glucose/lactate levels, samples were pooled between two and three Transwells, and pooled samples were counted as single replicates. Otherwise, replicates indicate unique Transwells for biochemical analysis and fields of view for microscopy analysis. All figures in this article represent either individual data points or the arithmetic mean ± standard error unless otherwise noted. Western blot and immunocytochemistry data were analyzed with one-way ANOVA or a Student's *t*-test. OCR and metabolic flux data were analyzed by a one-way ANVOA, using Dunnett's multiple comparisons test for individual significance values. All significance was tested against the "normal" condition, which is either a 200-µL apical medium volume or 21% O_2. *P* values are listed within each figure panel. The significance threshold for statistical tests was $P \leq 0.05$. All statistics were calculated using Prism v9.5.0 (GraphPad Software, La Jolla, CA, USA).

Results

Cell Culture Medium Volume Determines the Balance Between Hypoxic Conditions and Nutrient Availability, With Only Subtle Effects on Markers of RPE Health

hfRPE and iPSC-RPE cultures were grown on Transwell filters to best mimic cellular polarity and access to nutrients in vivo. The apical side of the filter faces the air–medium interface, and the basal surface faces the bottom of the culture plate. We have previously established these cultures as highly polarized and differentiated, with high TEER, expression of RPE-specific expression markers, high pigmentation, and capacity for photoreceptor outer segment (OS) phagocytosis.[25,27]

O_2 can reach cells through either chamber (Fig. 1A), but the apical chamber media directly touch cells without an intervening membrane and unrestricted access to the atmosphere, so we chose to alter apical media volumes to understand the effect of media volume on O_2 availability at the cell monolayer. We hypothesized that O_2 availability and therefore OCR are limited by medium depth under standard culture conditions, where apical medium volume can vary between 100 and 200 µL or more on 24-well Transwells, corresponding to a media column height varying between 3 and 6 mm. To test this hypothesis, we grew hfRPE or iPSC-RPE on 96-well plastic plates, which have the same surface area as a 24-well Transwell. We measured OCR in wells with 65, 95, 125, or 200 µL of media. The Resipher instrument determines OCR based on the vertical $[O_2]$-gradient that develops within the medium in the well. OCR is lowest at 200 µL (<100 fmol/mm^2/s) but increases with lower apical medium volumes (Figs. 1B, 1C; Supplementary Fig. S2), showing that OCR is indeed limited by medium volume. Initial steady-state OCR is nearly identical at depths corresponding to 65 µL and 95 µL of medium (150 fmol/mm^2/s for hfRPE; 180 fmol/mm^2/s for iPSC-RPE), suggesting that at volumes just under 100 µL, $[O_2]$ no longer limits oxidative phosphorylation (Figs. 1B, 1C; Supplementary Fig. S2). Given a cell culture surface area of 0.33 cm^2, this corresponds to a media volume to surface area ratio of 300 µL/cm^2. These OCR values, stable for almost a day, represent how the cultures initially respond to O_2 availability. With additional time, cells growing underneath higher columns of medium further adapt their OCR to limited O_2 availability.

Our data imply that human RPE cells could be hypoxic when grown at >300 µL/cm^2. To confirm that cells under higher columns of media sense hypoxia, we measured levels of the hypoxia responsive transcription factor, HIF-1α. HIF-1α is degraded when hydroxylated, and the ability of cells to hydroxylate HIF-1α depends on the availability of O_2.[33] Thus, low O_2 concentrations increase HIF-1α levels. We treated hfRPE on Transwells at 8% atmospheric or 21% atmospheric O_2 for 24 hours and, at each atmospheric O_2 concentration, also modulated apical medium volume, while maintaining basolateral media volume constant at 400 µL. Western blot of hfRPE lysate revealed a clear effect of both medium depth and of atmospheric $[O_2]$ on HIF-1α, supporting the conclusion that increasing medium volumes can lead to hypoxia in culture (Fig. 1D). Notably, while 8% O_2 is considered physioxic in vivo, 8% atmospheric O_2 increases HIF-1α levels in vitro. Even under the lowest culture volume, 65 µL, HIF-1α was significantly more stabilized in the 8% O_2 conditions than the 21% O_2 conditions (Fig. 1D, bottom right). This reaffirms that high diffusion distance in vitro limits O_2 access to cells and complicates comparisons of O_2 concentrations in vivo with O_2 concentrations in vitro.

While lower media volumes improve O_2 availability, they may also limit nutrient supply by increasing the rate at which mitochondria use metabolic fuels in medium and by decreasing the total moles of nutrient available to cells. The typical interval between medium changes in RPE cultures is 48 to 72 hours. To measure the effects of media volume on substrate depletion rates, we supplied 65, 95, 125, or 200 µL medium to hfRPE or iPSC-RPE and measured OCR up to 120 hours. When all mitochondrial substrates have been consumed, OCR will drop. With 65 µL, the time to a 50% drop for hfRPE from steady-state OCR was 76.7 ± 1.3 (mean ± SEM) hours after a medium change. With 95 µL, OCR dropped to 50% by 109 ± 4.2 hours after a medium change. At greater medium depths, OCR persisted at steady-state levels past 120 hours. Thus, at media volumes just under a ratio of 300 µL/cm^2, hfRPE grows without O_2 limitation and requires media changes just twice weekly to prevent a significant decrease in OCR from insufficient fuel availability (Fig. 1E). Similar trends were observed for iPSC-RPE, although the cultures could tolerate proportionately longer times between media changes without an OCR drop from nutrient depletion (Supplementary Fig. S2).

To determine the effects of media volume on typical markers of RPE health, we examined tight-junction integrity, morphology, and pigmentation.[34] We previously established TEER as a sensitive marker for subtle cell death.[35] hfRPE cultures supplied with 100 µL or 200 µL of media for up to 3 weeks had no differences in cell morphology or pigmentation (Supplementary Fig. S3A) and only subtle differences in TEER, present only after exposure for 3 weeks and not 1 week (Supplementary Fig. S3B). These results suggest that many aspects of RPE physiology in high media-volume cultures can continue without meaningful disruption, despite profound metabolic changes.

Investigative Ophthalmology & Visual Science

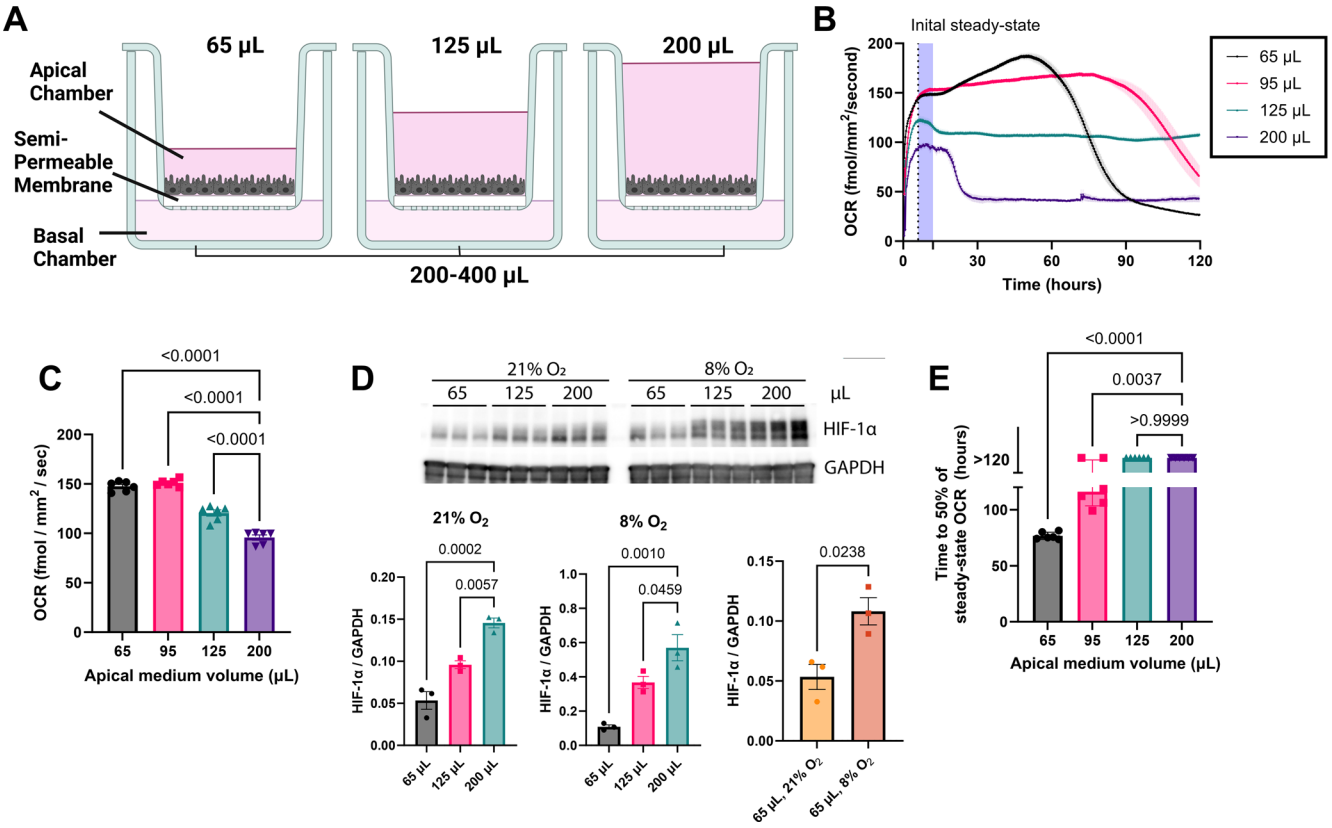

Figure 1. Medium depth limits cellular O_2 uptake by increasing O_2 diffusion distance. (**A**) Schematic showing the path O_2 must take to get from air, through liquid barriers (culture medium), and to cells at varying apical volumes and constant basal volume. (**B**) OCR over time for wells at different medium depths (65, 95, 125, 200 µL; $n = 6$ wells/group, donor 1). Results replicated with two additional hfRPE donors and two iPSC-RPE donors (Supplementary Fig. S2), for a total of five donors across two RPE cell culture types. (**C**) Average initial steady-state OCR (as designated in **B**) at each medium depth. (**D**) [O_2]-dependent or medium volume-dependent changes in HIF-1α, as assessed by Western blot (normalized to GAPDH) ($n = 3$, donor 2). (**E**) Medium volume also affects mitochondrial fuel availability. As these fuels are depleted, OCR drops. Plotted is time (in hours) after media change until OCR drops to 50% of steady state ($n = 6$, donor 1). All cultures are hfRPE. Data are represented as mean ± SEM.

Limiting O_2-Dependent Metabolism Accelerates Glycolysis, Depleting Glucose Faster and Causing an Accumulation of Lactate

When O_2 availability limits mitochondrial metabolism, cells can process glucose by reducing pyruvate into lactate. This mode of glucose utilization produces ATP at ~1/16th the efficiency as complete oxidation of glucose to CO_2 by fully coupled mitochondria, so more glucose is consumed to support the same energetic needs.

We examined the effects of limiting O_2 availability on glucose consumption and lactate production in hfRPE cultures. We cultured cells on Transwells with 100 µL apical medium and 200 µL basolateral media over 24 hours, where the cells were equilibrated with 21% O_2 in air. Next, we incubated the same cells in the same media volume but set O_2 at 8% in air. We measured total glucose and total lactate content in culture medium before it was exposed to cells and after 24 hours with enzymatic assays. The 8% O_2 increased glucose utilization (Fig. 2A) and lactate production (Fig. 2B) such that almost all glucose provided to RPE cells was consumed by 24 hours.

To determine whether higher medium volumes have the same effect on glucose consumption and lactate production as 8% O_2, we cultured hfRPE in ambient O_2 (21%) for 22 hours in 65, 125, or 200 µL of apical media and 400 µL of media basolaterally. We replaced 5 mM unlabeled glucose with 5 mM $^{13}C_6$-glucose and supplemented medium with 150 µM palmitate–BSA and 150 µM oleate–BSA to provide mitochondrial substrates. We probed metabolite release into the apical and basal chambers through a combination of mass spectrometry and enzymatic assays.

Like when cells are cultured at a low O_2 concentration, RPE cell glucose consumption (Figs. 2C, 2D) and lactate production (Figs. 2E, 2F) from 4 to 22 hours increased with greater apical medium depth. Qualitatively similar results were replicated in human iPSC-RPE cultures (Supplementary Fig. S4). For the first 4 hours after a medium change, glycolytic flux was insensitive to apical medium depth, and differences between conditions only appeared between 4 and 22 hours in culture. This latency required to detect changes in glycolysis likely occurred because O_2 gradients take time to develop, and flux differed only after steady-state O_2 gradients formed, triggering hypoxia. This hypothesis is supported by measurements of O_2 concentration 1 mm above the RPE monolayer, which showed that O_2 availability was progressively more limited after several hours in culture, and higher apical medium volumes further decreased [O_2] above cells (Fig. 2G). While there was a large decrease over time in

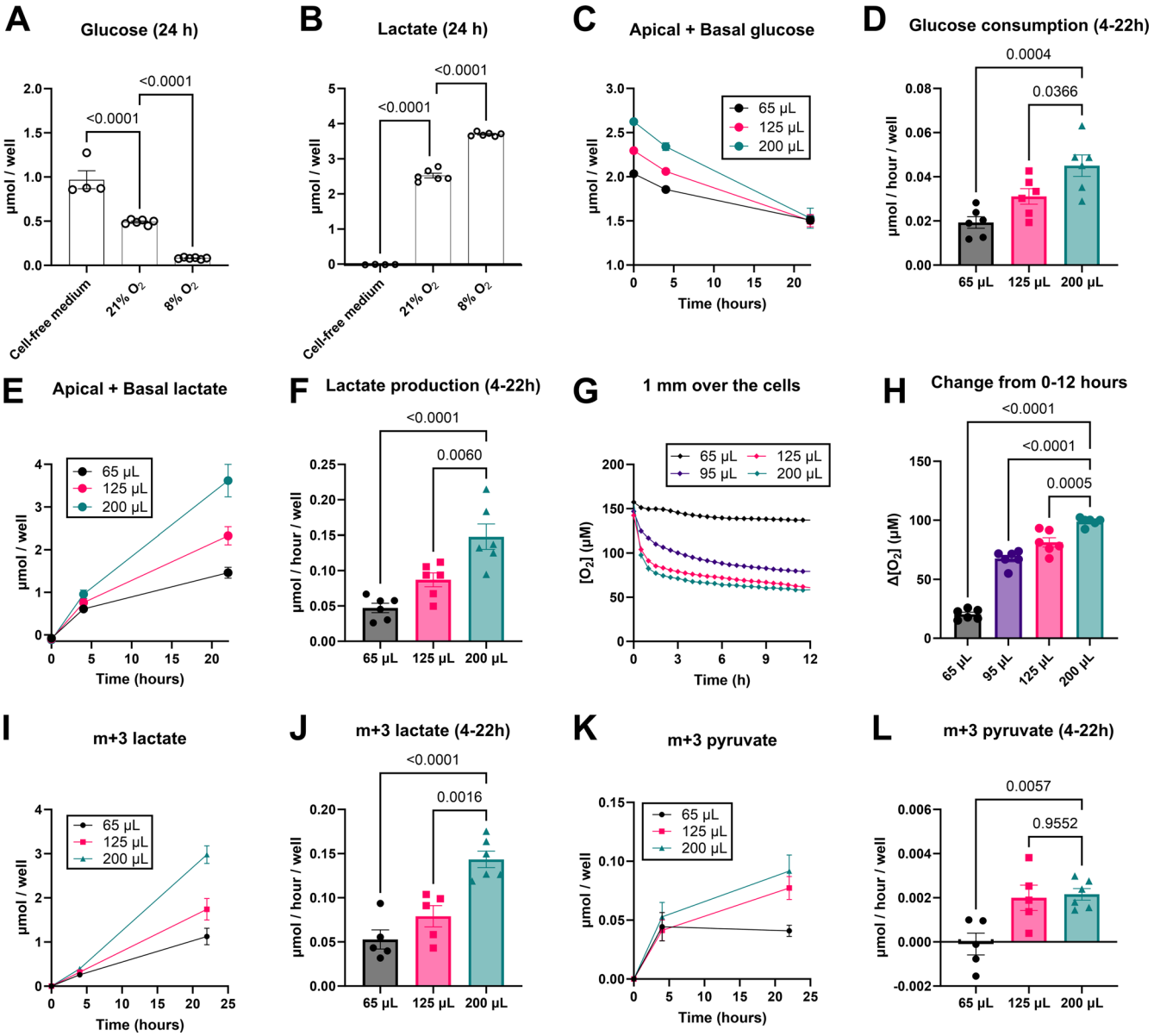

Figure 2. Glycolysis is accelerated by increasing medium depth. (**A**) Medium glucose and (**B**) medium lactate amounts after 24 hours of culture in medium without cells, medium with cells at 21% atmospheric O_2, or cells at 8% atmospheric O_2. Decreased O_2 levels increase glucose utilization and lactate production ($n = 6$, donor 2). Increasing medium volume also limits cellular O_2 availability, increasing glucose consumption (**C** shows total glucose levels over time and **D** is the quantified consumption rate from 4–22 hours) and lactate production (**E** shows lactate levels over time and **F** is the quantified production rate from 4–22 hours) ($n = 6$, donors 3, 4, and 5). (**G**) Limited cellular O_2 availability develops only after several hours in culture as steady-state O_2 diffusion gradients develop. This explains why medium volume effects on glucose and lactate (**C–F**) develop only after 4 hours. The graph shows the drop in medium $[O_2]$ 1 mm above the cells following a media change. (**H**) Change in $[O_2]$ 1 mm over cells during the first 12 hours after media change, confirming marked drops in O_2 availability only (i) with higher media column heights and (ii) after several hours in culture ($n = 6$, donor 1). (**I–L**) $^{13}C_6$-glucose tracing demonstrates increased m+3 lactate (**I–J**) and m+3 pyruvate (**K–L**) production with higher media column heights, confirming higher glycolysis rates with higher media volumes and mimicking trends in unlabeled lactate production from **E** to **F** ($n = 5–6$, donors 3, 4, and 5). All cultures are hfRPE and all metabolite analyses were done from media pooled from apical and basal chambers.

steady-state $[O_2]$ 1 mm over cells at higher medium volumes, that change was significantly blunted at lower medium volumes because O_2 had to diffuse a much shorter distance from atmosphere to reach the same 1-mm point above cells (Fig. 2H).

Pyruvate and other fuels already in culture medium could be sources of lactate production, so total lactate production could reflect a different biological phenomenon than we originally anticipated. To follow carbons from glucose specifically, we quantified m+3 glycolytic products derived from $^{13}C_6$-glucose. After a steady-state O_2 gradient was established in culture (4 hours), m+3 lactate (Figs. 2I, 2J) and m+3 pyruvate (Figs. 2K, 2L) both increased in an apical volume–dependent manner. This indicates an acceleration in glycolysis as medium depth increased.

Investigative Ophthalmology & Visual Science

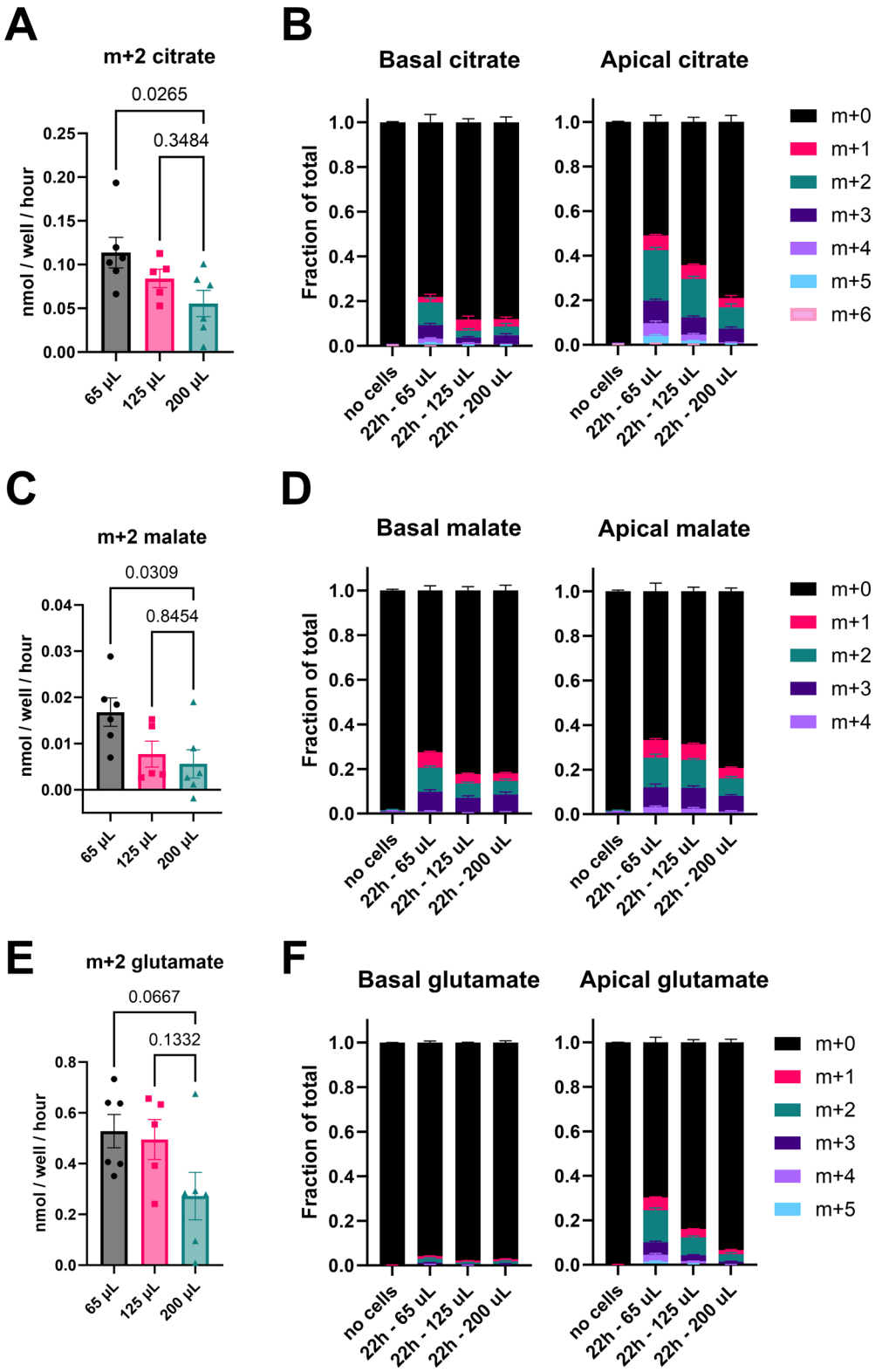

Figure 3. Mitochondrial activity increases with decreasing medium depth. We traced the incorporation of $^{13}C_6$-glucose into mitochondrial intermediates in hfRPE, measuring the rate of appearance of m+2 labeled intermediates in pooled apical + basal media from 4 to 22 hours after media change (**A**, **C**, **E**), as well as the fraction of each intermediate in the apical versus basolateral media that picked up a ^{13}C label at 22 hours (**B**, **D**, **F**). The apical media secretion rate of citrate (**A**), malate (**C**), and (**E**) glutamate derived from glucose (m+2) decreases with higher media volumes. In addition, the fraction of total (**B**) citrate, (**D**) malate, and (**F**) glutamate with a ^{13}C label decreases at higher media volumes. These results confirm that limited O_2 diffusion to cells prevents ongoing mitochondrial activity (n = 5–6, donors 3, 4, and 5).

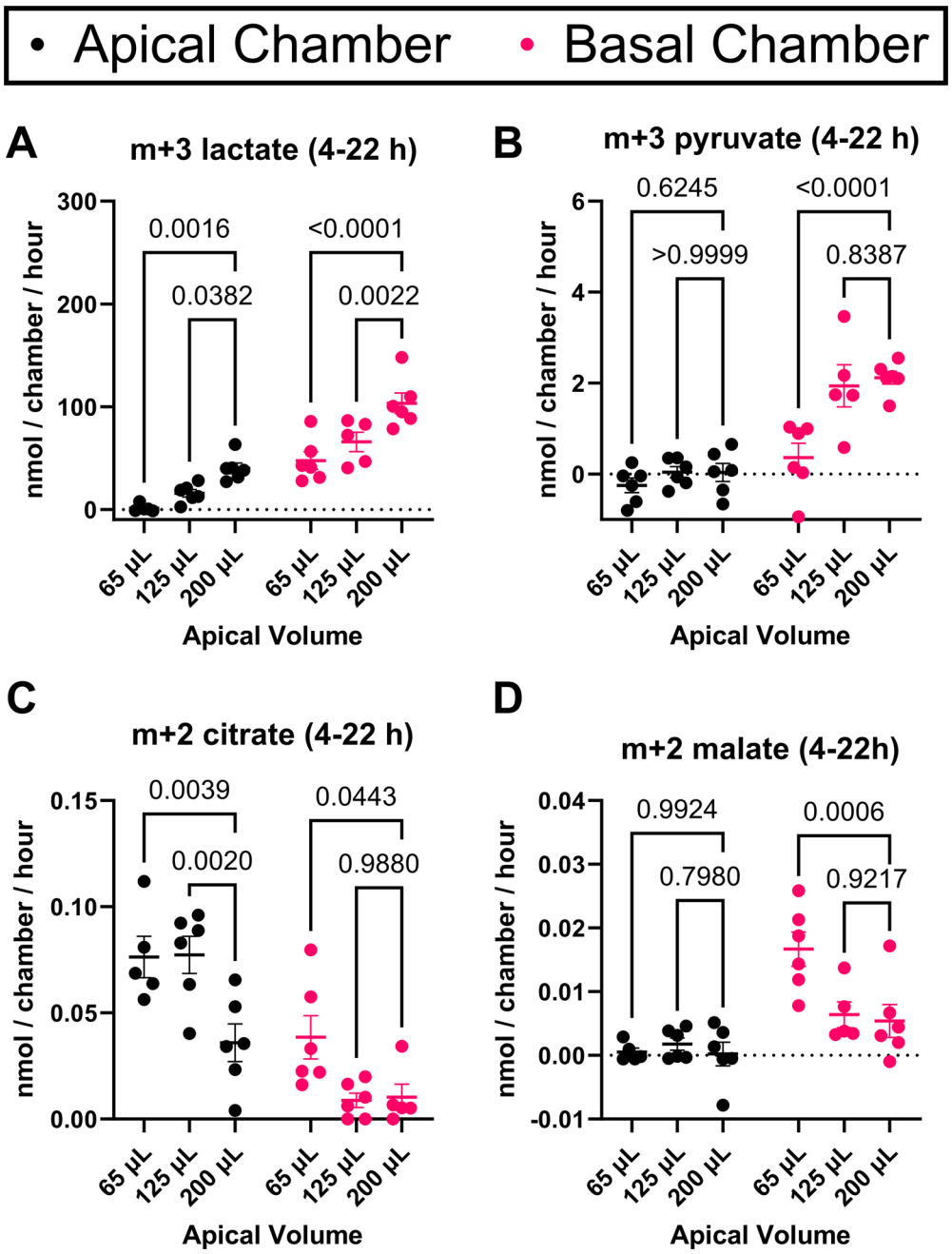

Figure 4. Volume effects on metabolite release rates depend on O_2 availability and mass action. While apical media volumes differ, basal media volumes are constant across all conditions, so release of metabolites into the basolateral media will be unaffected by mass action. (**A**) The release rate of m+3 lactate derived from $^{13}C_6$-glucose into the apical (*black dots*) or basal (*pink dots*) chambers from 4 to 22 hours in hfRPE is similarly affected by apical media volume, confirming O_2 availability is the dominant factor affecting release. Similar analysis for (**B**) m+3 pyruvate, also derived from glycolysis, where only basally secreted pyruvate is affected. (**C**, **D**) Particularly on the basal side, which is unaffected by mass action, mitochondrial intermediates from glucose are also affected by media volume: (**C**) m+2 citrate and (**D**) m+2 malate (n = 5–6, donors 3, 4, and 5).

Acetyl-CoA Utilization Increases With Decreasing Medium Depth

At lower apical medium volumes, more O_2 diffused to mitochondria, which should have facilitated mitochondrial TCA cycle activity and β-oxidation. Carbons from $^{13}C_6$-glucose were used in glycolysis to make m+3 pyruvate, which was then decarboxylated into m+2 acetyl-CoA. m+2 acetyl-CoA entered the TCA cycle and was incorporated into m+2 citrate and downstream m+2 intermediates. Labeled intermediates produced from acetyl-CoA were exported from cells into medium, so sampling media was a noninvasive way to assess metabolism of ^{13}C tracers.

Growing hfRPE on Transwells under conditions identical to those in Figure 2, we found a clear relationship between media depth and labeled intermediates released into media. As apical medium depth decreased, more m+2 citrate was made (Fig. 3A) and a greater proportion of citrate was ^{13}C-

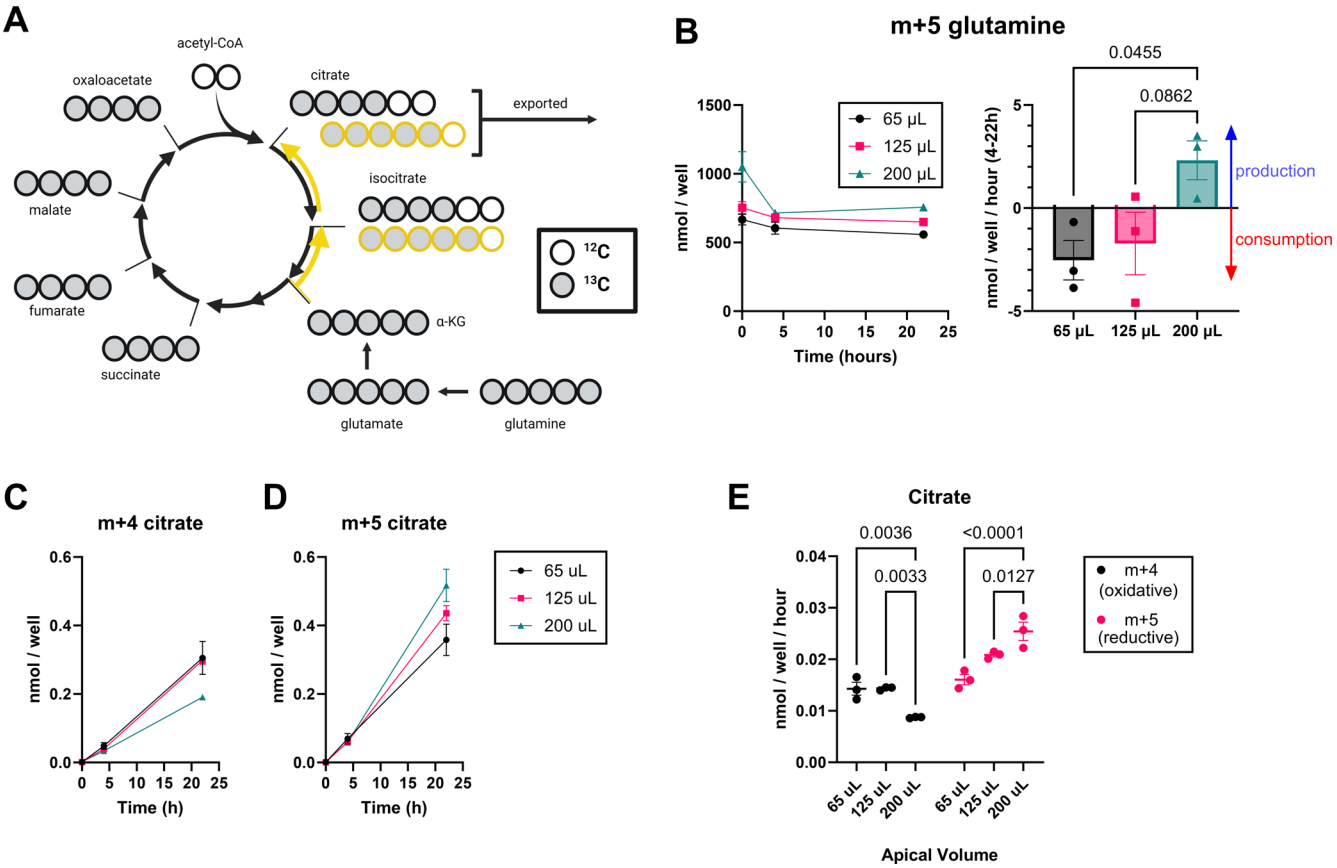

Figure 5. Reductive carboxylation of glutamine depends on medium depth. (**A**) Schematic detailing mitochondrial pathways for carbons from anapleurotic glutamine. These carbons enter the Krebs cycle as α-ketoglutarate and undergo either oxidative decarboxylation or reductive carboxylation. Both metabolic routes lead to the formation of citrate. If all carbons on glutamine are ^{13}C, reductive carboxylation leads to an m+5 citrate isotopologue, whereas oxidative decarboxylation leads to an m+4 citrate isotopologue. (**B**) In hfRPE culture, $^{13}C_5$-glutamine is marginally consumed at lower medium depths. (**C**, **D**) Tracing glutamine fate demonstrates that more is converted to citrate through oxidative decarboxylation at lower medium column heights (**C**) while more is converted to citrate through reductive carboxylation at higher medium column heights (**D**). (**E**) Quantification of oxidative versus reductive pathways from glutamine to citrate as a function of medium volume ($n = 3$, donor 6). Media pooled from apical and basal chambers for analysis.

labeled (Fig. 3B). The same trend existed for downstream TCA cycle and anapleurotic intermediates such as malate (Figs. 3C, 3D) and glutamate (Figs. 3E, 3F).

[O_2] Is the Driver of Differences in Metabolite Release Rates Between Different Volume Conditions

The law of mass action states that the driving force for a reaction is proportional to the relative concentrations of reactants and products. Applied to metabolite export into medium, this suggests that the ratio of the metabolite's intracellular and extracellular concentration will determine the driving force for export. Higher medium volumes dilute metabolites more and should increase the driving force for export. Thus, medium depth can affect cellular metabolism not only by altering cellular O_2 and nutrient availability but also through mass action. We tested whether this variable confounds the changes in secreted metabolites we observed from differences in O_2 supply.

While apical volumes in our experimental setup differed, basal volumes were constant. Thus, metabolite efflux to the basal side should reflect O_2-dependent differences in RPE metabolism. When labeling of lactate, pyruvate, citrate, and malate from $^{13}C_6$-glucose was measured separately in apical and basal chambers, there was a clear effect of volume on the export of m+3 lactate (Fig. 4A), m+3 pyruvate (Fig. 4B), m+2 citrate (Fig. 4C), and m+2 malate (Fig. 4D) in the basal chamber of hfRPE cultures. Glucose consumption and lactate production were also greater in the basal chamber of iPSC-RPE Transwell cultures when apical media were increased (Supplementary Fig. S4). The release rate of mitochondrial metabolites was inversely proportional to medium volume, consistent with less TCA cycle activity when the availability of O_2 was diminished.

Media Volume Affects RPE Reductive Carboxylation

Glutamine is the most abundant amino acid in serum, and it can be an anapleurotic TCA cycle intermediate. Glutamine imported into a cell can be converted to α-ketoglutarate (α-KG), which then can be metabolized by oxidative decarboxylation to succinyl-CoA or by reductive carboxylation to isocitrate and then citrate (Fig. 5A). Reductive carboxylation consumes reducing power that could be spent in the ETC,

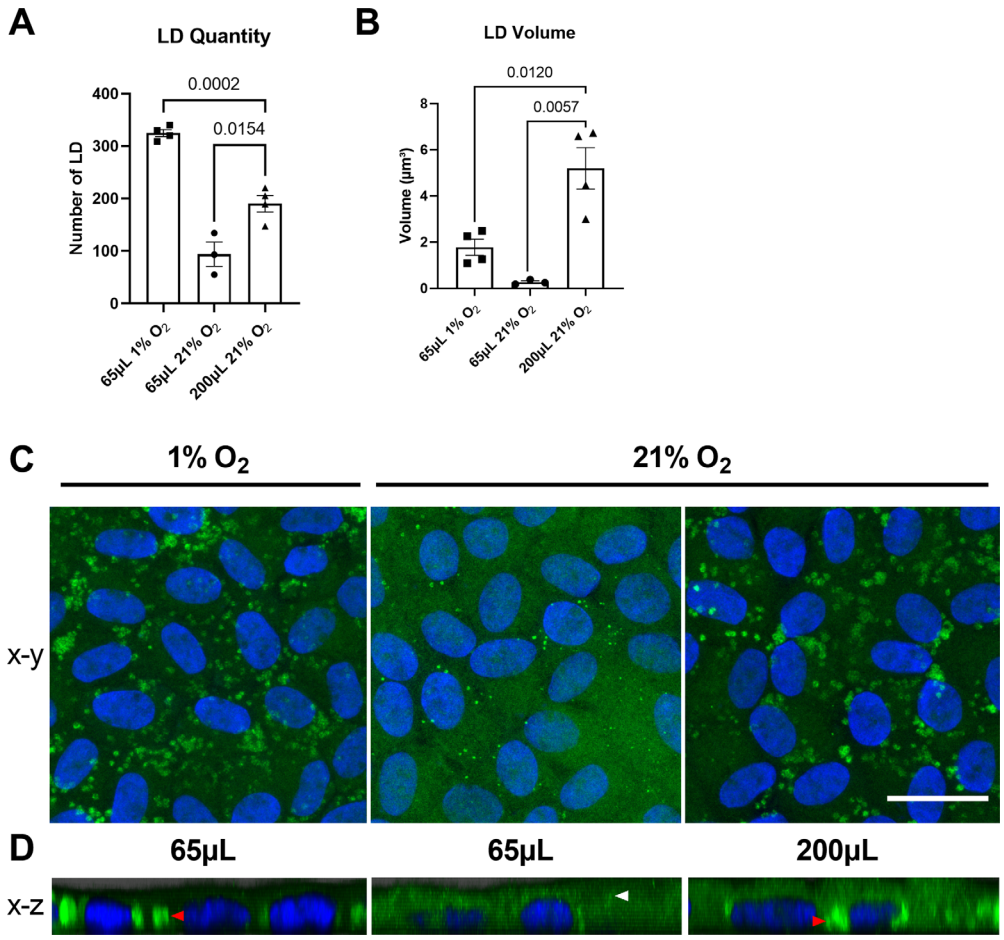

Figure 6. Medium depth affects RPE lipid droplet size, number, and localization after lipid challenge. In both hypoxic (1% O_2) and high media volume (200 µL) conditions, there is an increase in the (**A**) number of LDs and (**B**) size of LDs formed after an 18-hour lipid challenge (300 µM palmitate) in hfRPE (n = 3–4 randomly selected images). (**C**) Immunostaining LDs (ADRP/perilipin-2, *green*) and nuclei (Hoechst 34580, *blue*) under high volume or 1% O_2 conditions. (**D**) The larger LDs that form under high-volume or low atmospheric O_2 conditions are predominantly basolateral (*red arrowhead*), adjacent to nuclei. The smaller LDs that form under normoxia are more apically localized (*white arrowhead*). All results from donor 6, and replication of results in an iPSC-RPE donor and another hfRPE donor is in Supplementary Figure S6. *Scale bar*: 10 µm.

and the resulting citrate carbons can be used to synthesize fatty acids, particularly when cells are hypoxic.[36] A previous study showed that RPE cells in culture have high capacity for reductive carboxylation.[37] That study used $^{13}C_5$-glutamine, which can be used to distinguish citrate made by oxidative TCA cycle activity from citrate made by reductive carboxylation (Fig. 5A). We found that reductive carboxylation can be influenced by hypoxia resulting from high media volume.

We incubated hfRPE cultures in $^{13}C_5$-glutamine for 22 hours, collecting aliquots of medium at 0, 4, and 22 hours following the medium change. Cultures consumed only a small fraction of glutamine from 4 to 22 hours (Fig. 5B). However, in tracing the fate of consumed glutamine, it was apparent that medium volume determined whether glutamine was converted to citrate through oxidative or reductive routes (Figs. 5C, 5D). At higher medium volumes, more glutamine was carboxylated, matching data from previous studies demonstrating reductive carboxylation in the RPE.[37] However, as the apical volume decreased, there was a proportional decline in reductive carboxylation (decreasing m+5 citrate) and increase in oxidative decarboxylation (increasing m+4 citrate) (Fig. 5E). These findings suggest that reductive carboxylation is favored when O_2 availability becomes limiting.

Media Volume Affects RPE Lipid Droplet Dynamics

The RPE is a prolific consumer of lipids[38] and forms temporary LDs in response to high lipid concentrations.[39] The ability of cells to metabolize fatty acids from lipid droplets partly controls the size and persistence of LDs.[40] β-Oxidation of fatty acids requires O_2, so we hypothesized that higher media columns would limit β-oxidation and cause accumulation of LDs. To test this hypothesis, we fed hfRPE or iPSC-RPE serum-free media supplemented with 300 µM BSA-conjugated palmitate for 18 hours, comparing LD formation with low versus high apical columns (and a constant basal volume with 21% atmospheric O_2). As a control for limited O_2 availability but equal absolute amounts of palmitate, we also provided cells with low apical volume but under 1% atmospheric O_2. Both decreasing O_2 levels by 1% atmospheric O_2 or by higher media columns increased the

number of LDs and their size (Figs. 6A–6C; Supplementary Fig. S5). Larger LDs were more likely to be localized basolaterally (Fig. 6D; Supplementary Fig. S5). Thus, studies that explore the role of lipid metabolism and LDs in the RPE need to be particularly cognizant of media volume effects.

Discussion

While primary and iPSC-RPE culture models show great promise in recapitulating characteristics of RPE in health and disease, media volumes commonly employed for RPE culture can limit O_2 availability. This impacts everything from mitochondrial metabolism to activation of hypoxia-responsive transcription factors to lipid dynamics. These data mirror findings on the impact of media volume in adipocytes,[23] and they support a recently published review detailing concerns about O_2 availability when studying RPE metabolism in vitro.[41] Despite profoundly affecting the TCA cycle and lipid metabolism, higher media column heights caused little change in commonly employed markers for RPE health. There were no effects on RPE morphology and pigmentation and only minor effects on TEER even after 3 weeks. This decoupling of cellular metabolism from RPE function/survival could explain why effects of media volume on RPE cultures have largely gone unnoticed.

Despite the lack of overt effects of medium depth on many markers of RPE culture health, it is essential that RPE metabolism be modeled accurately. HIF-1α is stabilized in media volumes often employed for RPE culture, yet given HIF's documented role in various RPE pathologies,[42–44] investigating RPE biology under conditions that constitutively activate HIF could be misleading. Numerous studies have established that LDs increase dramatically under hypoxia or conditions that activate HIF.[43,45] In our cultures, limited O_2 availability caused by greater medium depth altered LD number, size, and polarized intracellular localization after lipid challenge. Our findings are consistent with other studies showing hypoxia can increase LD size.[46]

The pathogenesis of AMD may involve RPE lipid handling, so there is intense interest in manipulating the RPE's management of its lipid load for therapeutic gain.[47] Given the very high demand for O_2 with β-oxidation, studies manipulating RPE fatty acid metabolism as a therapeutic pathway in AMD should be particularly careful to take into account effects of media volume.

In elucidating metabolic pathways affected by the height of the media column, we found that the RPE utilizes reductive carboxylation of glutamine mainly under hypoxic conditions. Prior studies[37] had suggested that the RPE is uniquely capable of reductive carboxylation as a mechanism for maintaining antioxidant defense. We suggest that when O_2 is available, the RPE engages in both the oxidative and reductive pathways to about the same extent, but during hypoxia, the reductive pathway predominates.

Cellular O_2 availability depends not just on media depth but also on the cell monolayer's OCR. When OCR is higher, O_2 is depleted faster and lower media depths are necessary to ensure adequate O_2 supply. In this study, hfRPE and iPSC-RPE OCR necessitate a volume/surface area ratio of 300 µL/cm^2 or lower to avoid hypoxia at the cell monolayer. Media volume to surface area ratios lower than 300 µL/cm^2 would increase O_2 availability but are not necessary because they do not further increase OCR and could restrict nutrient availability. At a volume/surface area ratio of approximately 200 µL/cm^2 (65 µL in a 24-well Transwell, 220 µL in a 12-well Transwell), nutrient depletion *begins* to affect mitochondrial metabolism after 2 to 4 days, whereas at a ratio of approximately 300 µL/cm^2 (95 µL in a 24-well Transwell, 425 µL in a 12-well Transwell), nutrient depletion does not *begin* to affect mitochondrial metabolism until 4 days or more (Fig. 1B; Supplementary Fig. S2). Since most labs change cell culture media between two and three times per week, a volume/surface area ratio of approximately 300 µL/cm^2 balances O_2 supply and nutrient availability for hfRPE. One caveat to this general advice is that when O_2 demand increases above baseline (e.g., during experiments involving mitochondrial uncoupling or when β-oxidation is stimulated), media volume levels lower than 300 µL/cm^2 are necessary to facilitate the process being studied. We have found, for example, that β-oxidation of exogenously added palmitate to hfRPE cultures proceeds more quickly and efficiently at media volumes of 200 µL/cm^2 compared to a volume of 300 µL/cm^2 (Supplementary Fig. S6).

Factors other than media depth and OCR also influence O_2 availability in vitro. These include diffusion of O_2 through the plastic sides and bottom surface of the well, humidity in the incubator, and the atmospheric pressure (e.g., in labs at elevation).[24] These effects can be controlled only partially, but they can be compensated for by altering medium volume. To estimate the consequences of manipulating medium volume and other parameters on cellular O_2 availability, we designed an interactive web notebook, available at https://observablehq.com/@lucid/oxygen-diffusion-and-flux-in-cell-culture. The assumptions and calculations underpinning this calculator are outlined in the Supplementary Discussion.

In conclusion, media depth is a critical factor that determines availability of O_2 in RPE culture, with myriad serious consequences disguised behind normal-appearing morphology and pigmentation. As the RPE depends on mitochondrial function in vivo and certain RPE-centric diseases involve highly O_2-consumptive processes such as lipid oxidation, avoiding media volumes that limit O_2 in vitro will more faithfully replicate RPE behavior in vivo.[4–8,11–13,38,47] Unfortunately, medium volume has been reported only rarely in studies using RPE cell culture, including our own prior publications. To ensure more consistency across studies of RPE metabolism and mitochondrial health, we recommend reporting cell culture surface area, confluency, media volume, and time between media change and the end point of the experiment.[24] For RPE cultures with OCR rates similar to hfRPE and iPSC-RPE, we recommend maintaining cultures at no more than 300 µL of media per cm^2 of surface area with no more than 4 days between media changes, and for biological processes predicted to involve O_2 consumption above baseline, volumes $\leq$200 µL/cm^2 with media changes every other day may be needed.

Acknowledgments

Figures 1A and 5A were created with BioRender.com. The authors thank Subramanian Pennathur for helpful comments and Abby Fahim and Dayanthi Perera for help with iPSC-RPE cultures.

Supported by a career development grant by the National Eye Institute (K08EY033420) to JMLM, the James Grosfeld Initiative for Dry AMD (https://jasonmiller.lab.medicine.umich.edu/links), the Dee and Dickson Brown Vision Care and Research Fund, a Brightfocus Foundation Postdoctoral Fellowship (M2022003F) to DTH, and NEI RO1EY06641, RO1EY017863,

and R21032597, as well as Foundation Fighting Blindness TA-NMT-0522-0826-UWA-TRAP to JBH. No federal funds were used for prenatal tissue research.

Disclosure: **D.T. Hass**, None; **Q. Zhang**, None; **G.A. Autterson**, None; **R.A. Bryan**, None; **J.B. Hurley**, None; **J.M.L. Miller**, None

References

1. Swarup A, Samuels IS, Bell BA, et al. Modulating GLUT1 expression in retinal pigment epithelium decreases glucose levels in the retina: impact on photoreceptors and Müller glial cells. *Am J Physiol Cell Physiol*. 2019;316(1):C121–C133.
2. Lakkaraju A, Umapathy A, Tan LX, et al. The cell biology of the retinal pigment epithelium. *Prog Retin Eye Res*. 2020;78:100846.
3. Chowers G, Cohen M, Marks-Ohana D, et al. Course of sodium iodate-induced retinal degeneration in albino and pigmented mice. *Invest Ophthalmol Vis Sci*. 2017;58(4):2239–2249.
4. Latvala T, Mustonen E, Uusitalo R, Majamaa K. Pigmentary retinopathy in patients with the MELAS mutation 3243A–>G in mitochondrial DNA. *Graefes Arch Clin Exp Ophthalmol*. 2002;240(10):795–801.
5. Tsang SH, Aycinena ARP, Sharma T. Mitochondrial disorder: maternally inherited diabetes and deafness. *Adv Exp Med Biol*. 2018;1085:163–165.
6. Zhao C, Yasumura D, Li X, et al. mTOR-mediated dedifferentiation of the retinal pigment epithelium initiates photoreceptor degeneration in mice. *J Clin Invest*. 2011;121(1):369–383.
7. Ferrington DA, Fisher CR, Kowluru RA. Mitochondrial defects drive degenerative retinal diseases. *Trends Mol Med*. 2020;26(1):105–118.
8. Kaarniranta K, Uusitalo H, Blasiak J, et al. Mechanisms of mitochondrial dysfunction and their impact on age-related macular degeneration. *Prog Retin Eye Res*. 2020;79:100858.
9. Kanow MA, Giarmarco MM, Jankowski CS, et al. Biochemical adaptations of the retina and retinal pigment epithelium support a metabolic ecosystem in the vertebrate eye. *Elife*. 2017;6.
10. Bisbach CM, Hass DT, Robbings BM, et al. Succinate can shuttle reducing power from the hypoxic retina to the O2 rich pigment epithelium. *Cell Rep*. 2020;31(5):107606.
11. Fisher CR, Ferrington DA. Perspective on AMD pathobiology: a bioenergetic crisis in the RPE. *Invest Ophthalmol Vis Sci*. 2018;59(4):AMD41–AMD47.
12. Reyes-Reveles J, Dhingra A, Alexander D, Bragin A, Philp NJ, Boesze-Battaglia K. Phagocytosis-dependent ketogenesis in retinal pigment epithelium. *J Biol Chem*. 2017;292(19):8038–8047.
13. Adijanto J, Du J, Moffat C, Seifert EL, Hurle JB, Philp NJ. The retinal pigment epithelium utilizes fatty acids for ketogenesis. *J Biol Chem*. 2014;289(30):20570–20582.
14. Mitchell P. Coupling of phosphorylation to electron and hydrogen transfer by a chemi-osmotic type of mechanism. *Nature*. 1961;191:144–148.
15. Adijanto J, Philp NJ. Cultured primary human fetal retinal pigment epithelium (hfRPE) as a model for evaluating RPE metabolism. *Exp Eye Res*. 2014;126:77–84.
16. Bharti K, den Hollander AI, Lakkaraju A, et al. Cell culture models to study retinal pigment epithelium-related pathogenesis in age-related macular degeneration. *Exp Eye Res*. 2022;222:109170.
17. Galloway CA, Dalvi S, Hung SSC, et al. Drusen in patient-derived hiPSC-RPE models of macular dystrophies. *Proc Natl Acad Sci USA*. 2017;114(39):E8214–E8223.
18. George A, Sharma R, Pfister T, et al. In vitro disease modeling of oculocutaneous albinism type 1 and 2 using human induced pluripotent stem cell-derived retinal pigment epithelium. *Stem Cell Reports*. 2022;17(1):173–186.
19. Rabin DM, Rabin RL, Blenkinsop TA, Temple S, Stern JH. Chronic oxidative stress upregulates Drusen-related protein expression in adult human RPE stem cell-derived RPE cells: a novel culture model for dry AMD. *Aging (Albany NY)*. 2013;5(1):51–66.
20. Zhang Q, Presswalla F, Calton M, et al. Highly differentiated human fetal RPE cultures are resistant to the accumulation and toxicity of lipofuscin-like material. *Invest Ophthalmol Vis Sci*. 2019;60(10):3468–3479.
21. Zhang Q, Presswalla F, Ali RR, Zacks DN, Thompson DA, Miller JML. Pharmacologic activation of autophagy without direct mTOR inhibition as a therapeutic strategy for treating dry macular degeneration. *Aging (Albany NY)*. 2021;13(8):10866–10890.
22. Linsenmeier RA, Zhang HF. Retinal oxygen: from animals to humans. *Prog Retin Eye Res*. 2017;58:115–151.
23. Tan J, Virtue S, Norris DM, et al. Oxygen is a critical regulator of cellular metabolism and function in cell culture. *bioRxiv*. 2022:2022.11.29.516437.
24. Al-Ani A, Toms D, Kondro D, Thundathil J, Yu Y, Ungrin M. Oxygenation in cell culture: critical parameters for reproducibility are routinely not reported. *PLoS One*. 2018;13(10):e0204269.
25. Zhang Q, Presswalla F, Feathers K, et al. A platform for assessing outer segment fate in primary human fetal RPE cultures. *Exp Eye Res*. 2019;178:212–222.
26. Maminishkis A, Chen S, Jalickee S, et al. Confluent monolayers of cultured human fetal retinal pigment epithelium exhibit morphology and physiology of native tissue. *Invest Ophthalmol Vis Sci*. 2006;47(8):3612–3624.
27. Chen L, Perera ND, Karoukis AJ, et al. Oxidative stress differentially impacts apical and basolateral secretion of angiogenic factors from human iPSC-derived retinal pigment epithelium cells. *Sci Rep*. 2022;12(1):12694.
28. Fernandes M, McArdle B, Schiff L, Blenkinsop TA. Stem cell-derived retinal pigment epithelial layer model from adult human globes donated for corneal transplants. *Curr Protoc Stem Cell Biol*. 2018;45(1):e53.
29. Sharma R, Bose D, Montford J, Ortolan D, Bharti K. Triphasic developmentally guided protocol to generate retinal pigment epithelium from induced pluripotent stem cells. *STAR Protoc*. 2022;3(3):101582.
30. Seidemann J, Lowry OH, Und JV. Passonneau: a flexible system of enzymatic analysis. Academic Press, New York, 1972. 291 S., 32 Abb., 15 Tab., Preis $ 14.00. *Starch Stärke*. 1973;25(9):322.
31. Du J, Rountree A, Cleghorn WM, et al. Phototransduction influences metabolic flux and nucleotide metabolism in mouse retina. *J Biol Chem*. 2016;291(9):4698–4710.
32. Millard P, Delépine B, Guionnet M, Heuillet M, Bellvert F, Létisse F. IsoCor: isotope correction for high-resolution MS labeling experiments. *Bioinformatics*. 2019;35(21):4484–4487.
33. Safran M, Kaelin WG. HIF hydroxylation and the mammalian oxygen-sensing pathway. *J Clin Invest*. 2003;111(6):779–783.
34. Schaub NJ, Hotaling NA, Manescu P, et al. Deep learning predicts function of live retinal pigment epithelium from quantitative microscopy. *J Clin Invest*. 2020;130(2):1010–1023.
35. Miller JML, Zhang Q, Johnson MW. Regression of drusen or vitelliform material heralding geographic atrophy: correlation between clinical observations and basic science. *Graefes Arch Clin Exp Ophthalmol*. 2021;259(7):2051–2053.
36. Metallo CM, Gameiro PA, Bell EL, et al. Reductive glutamine metabolism by IDH1 mediates lipogenesis under hypoxia. *Nature*. 2011;481(7381):380–384.

Investigative Ophthalmology & Visual Science

37. Du J, Yanagida A, Knight K, et al. Reductive carboxylation is a major metabolic pathway in the retinal pigment epithelium. *Proc Natl Acad Sci USA*. 2016;113(51):14710–14715.
38. Lewandowski D, Sander CL, Tworak A, Gao F, Xu Q, Skowronska-Krawczyk D. Dynamic lipid turnover in photoreceptors and retinal pigment epithelium throughout life. *Prog Retin Eye Res*. 2022;89:101037.
39. Baker BN, Moriya M, Maude MB, Anderson RE, Williams TP. Oil droplets of the retinal epithelium of the rat. *Exp Eye Res*. 1986;42(6):547–557.
40. Rambold AS, Cohen S, Lippincott-Schwartz J. Fatty acid trafficking in starved cells: regulation by lipid droplet lipolysis, autophagy, and mitochondrial fusion dynamics. *Dev Cell*. 2015;32(6):678–692.
41. Yazdani M. Uncontrolled oxygen levels in cultures of retinal pigment epithelium: have we missed the obvious? *Curr Eye Res*. 2022;47(5):651–660.
42. Kong Y, Liu PK, Li Y, et al. HIF2α activation and mitochondrial deficit due to iron chelation cause retinal atrophy. *EMBO Mol Med*. 2023;15(2):e16525.
43. Kurihara T, Westenskow PD, Gantner ML, et al. Hypoxia-induced metabolic stress in retinal pigment epithelial cells is sufficient to induce photoreceptor degeneration. *Elife*. 2016;5.
44. Kurihara T, Westenskow PD, Friedlander M. Hypoxia-inducible factor (HIF)/vascular endothelial growth factor (VEGF) signaling in the retina. *Adv Exp Med Biol*. 2014;801:275–281.
45. Boström P, Magnusson B, Svensson PA, et al. Hypoxia converts human macrophages into triglyceride-loaded foam cells. *Arterioscler Thromb Vasc Biol*. 2006;26(8):1871–1876.
46. de la Rosa Rodriguez MA, Kersten S. Regulation of lipid droplet homeostasis by hypoxia inducible lipid droplet associated HILPDA. *Biochim Biophys Acta Mol Cell Biol Lipids*. 2020;1865(9):158738.
47. Jun S, Datta S, Wang L, Pegany R, Cano M, Handa JT. The impact of lipids, lipid oxidation, and inflammation on AMD, and the potential role of miRNAs on lipid metabolism in the RPE. *Exp Eye Res*. 2019;181:346–355.

Investigative Ophthalmology & Visual Science